Published in final edited form as:
J Immunol Methods. 2010 April 15; 355(1-2): 1–13. doi:10.1016/j.jim.2010.02.003.

Quantitative measurement of F-actin accumulation at the NK cell immunological synapse

Pinaki P. Banerjee[1] and **Jordan S. Orange**[1,2]

[1]The Children's Hospital of Philadelphia Research Institute, 3615 Civic Center Blvd., Philadelphia, PA 19104 USA

Abstract

NK cells are lymphocytes of the innate immune system that can kill target cells after activation signal-induced directional secretion of lytic granule contents. This process depends upon F-actin polymerization at the NK cell immunological synapse (NKIS), which is the dynamic organization of molecules at the interface between the NK cell and target cell. Although F-actin accumulation at the NKIS is easily visualized, the ability to quantify F-actin at the NKIS is required to understand how F-actin reorganization and accumulation enable NK cell function. Here, we demonstrate several novel algorithms for measuring the content of F-actin accumulated at the NKIS with special emphasis upon actin contributed by the NK cell. These algorithms do not rely upon overexpressing fluorescent proteins or preincubating cells with vital fluorescent dyes. Using models of the activating and inhibitory NKIS as well as NK cells expressing fluorescent protein - cell surface receptor fusion proteins, these algorithms were tested and were used to quantitatively demonstrate that F-actin accumulates at the activating, but not at the inhibitory NKIS. With these approaches, we have also established mathematical formulas that should prove valuable in the comprehensive quantitative evaluation of the NKIS and be more broadly applicable in the measurement of the accumulation of any fluorophore at an intercellular junction.

Keywords

NK cells; immunological synapse; F-actin; confocal microscopy; quantitative imaging

1) Introduction

1.1) The NK cell immunological synapse

The immunological synapse can be defined as the interface between an immune cell and the cell with which it interacts and has the potential to facilitate signal transduction events to enable immunological functions (Davis and Dustin, 2004). A specialized immunological synapse formed between an NK cell and its target is referred to as the NK cell immunological synapse (NKIS) (reviewed in (Orange, 2008)). Here, NK cells can receive activating and inhibitory signals to ultimately form either an activating or inhibitory NKIS. The commitment to one or

2To whom correspondence should be addressed. Jordan S. Orange, University of Pennsylvania School of Medicine, Children's Hospital of Philadelphia, Division of Immunology, 3615 Civic Center Blvd, ARC-1016H, Philadelphia, PA 19104, (Voice) 267-426-5622, (Fax) 267-426-5727, orange@mail.med.upenn.edu.

the other depends upon the relative strength and integration of these signals (Almeida and Davis, 2006). The inhibitory NKIS is transient and results in rapid detachment from the target cell (Burshtyn et al., 2000). The activating NKIS induces NK cell function that can include the directed secretion of lytic granule contents to mediate cytotoxicity of the target cell (Liu et al., 2009). This latter type of NKIS is also referred to specifically as a lytic NKIS. NK cells form the lytic NKIS through a sequential progression of steps that involve coordinated function of cell surface receptors, signaling molecules, cytoskeletal proteins, and cellular organelles (reviewed in (Orange, 2008)). One of the earliest steps in the maturation of the lytic NKIS is the accumulation of filamentous (F)-actin at the synapse (Orange et al., 2003; Wulfing et al., 2003), which facilitates the formation of a surpramolecular activation cluster (SMAC). An F-actin rich peripheral SMAC (pSMAC) is required for the polarization of the microtubule organizing center (MTOC) along with lytic granules to the NKIS to allow for directed secretion of the lytic granule contents and cytotoxicity (Orange et al., 2003). The MTOC and microtubules are then required for the delivery of the lytic granules to the NKIS. Specifically, the blockade of microtubule function prevents lytic granule polarization to the NKIS without affecting F-actin accumulation at the pSMAC (Orange et al., 2003; Banerjee et al., 2007). Thus, F-actin accumulation is an early and critical event in maturation and function of the lytic NKIS. This is specifically exploited by the inhibitory NKIS, which appears to utilize inhibitory signaling to directly prevent maturation of a cytolytic NKIS by interfering with F-actin accumulation (Masilamani et al., 2006).

1.2) Quantification of molecular accumulation at the NKIS

Numerous studies of the NKIS have evaluated the accumulation of molecules at the synapse using confocal fluorescent microscopy of fixed conjugates between NK cells and their targets (Borszcz et al., 2003; Orange et al., 2003; Wulfing et al., 2003; Almeida and Davis, 2006; Masilamani et al., 2006; Banerjee et al., 2007). This has allowed consideration of molecular relocalization to and role in coordinating cell function of the NKIS. In some cases, the molecules under consideration are not expressed in the target cell, such as killer cell immunoglobulin-like receptor (KIR) family members, and thus any accumulation of KIR at the NKIS is contributed by the NK cell. This is unfortunately not the case for many signaling and cytoskeletal molecules, such as F-actin, as they are found both in the NK as well as the target cell. Given the critical nature of F-actin in the formation of the NKIS (Orange et al., 2003; Wulfing et al., 2003) this presents an obstacle to truly comprehending the intricacies of synapse maturation. An additional experimental challenge results from different types of target cells having different amounts of F-actin content in their cortex. For example, two commonly used NK cell target cell lines, the 721.221 Epstein Barr Virus-transformed B cell line and K562 erythroleukemia cell line contain reproducibly different quantities of cortical F-actin (unpublished observations). Although alternative approaches, such as using NK cells expressing vectors encoding GFP-actin, loading cells prior to conjugation with vital fluorescent dyes, or evaluation via transmission electron microscopy can facilitate detecting the content of F-actin that is contributed specifically by an NK cell at the NKIS, they present challenges. Electron micrographs are difficult to quantitate and evaluate through 3 dimensions. Attempts to express fluorescent molecule fusion proteins can be inefficient and overexpression of the fusion proteins has the potential to induce unintended cellular effects. Similarly, incubating cells with vital dyes prior to conjugation has the potential to alter their biological activity. Thus, confocal fluorescence microscopy of conjugates between NK cells and target cells that have been stained with fluorescent antibodies or probes after fixation persists as an essential tool for evaluating F-actin accumulation at and the biology of the NKIS.

Another challenge in the use of fluorescent microscopy to evaluate the NKIS relates to a limited ability to identify smaller or incremental changes in molecular accumulations. For example, if a particular experimental intervention did not prevent the accumulation of F-actin at the NKIS

but instead reduced the amount of F-actin accumulated by one-half, could it be detected? Although different studies have utilized various approaches to define molecular accumulation at the NKIS (Borszcz et al., 2003; Orange et al., 2003; Wulfing et al., 2003; Almeida and Davis, 2006; Masilamani et al., 2006; Banerjee et al., 2007; Liu et al., 2009), improved quantitative approaches to discern incremental changes could allow for better understanding of the influences upon temporospatial synapse formation and maturation.

In an effort to be able to apply increased sensitivity in studies of the NKIS, we have developed and evaluated several algorithms for measuring molecular accumulation at the synapse. Although these approaches should be generally applicable to the accumulation of any fluorescent signal at an immunological synapse, we applied and validated our algorithms by measuring the F-actin content in the activating and inhibitory NKIS in 2- or 3-dimensional images. While we utilized GFP-receptor fusion protein-expressing NK cells to validate our approach, we also attempted to estimate the specific contribution of F-actin to the NKIS by the NK cell in the conjugate without an additional dependence upon fluorescent dyes, fluorescent fusion proteins, or cell manipulations. Using these algorithms in NK cells that were not manipulated prior to conjugation, we quantitatively demonstrated that the F-actin content at the lytic NKIS was significantly greater than that found in the cortex of unconjugated NK cells or target cells. We also quantitatively demonstrated that F-actin accumulation at the lytic NKIS was more abundant than that found at the inhibitory NKIS.

2) Materials and Methods

2.1) NK cell preparation, NK cell and target cell lines

Leukocyte-enriched blood was obtained from volunteer donors and was used to prepare *ex vivo* NK cells by negative selection using the human NK cell isolation kit II (Miltenyi Biotec) as described (Banerjee et al., 2007). NK cell preparations contained >96% $CD56^+/CD3^-$ cells with less than 1% $CD3^+$ cells as determined by FACS using fluorophore-conjugated mAbs (BD Biosciences). All human samples were obtained with approval of the Institutional Review Board of the Children's Hospital of Philadelphia. The immortalized NK cell line YTS-KIR2DL1-GFP was the gift of Dr. D. Burshtyn, (Borszcz et al., 2003), and YTS CD2-GFP cells were previously generated and described elsewhere (Orange et al., 2003). HLA Cw3-, or Cw4-expressing 721.221 B lymphoblastoid cells (Fassett et al., 2001) and K562 erythroleukemia target cells lines with or without transduced CD86 (KT86, and K562, respectively) were used as target cells (Banerjee et al., 2007).

2.2) Confocal microscopy

Conjugates between effector and target cells at a 2:1 ratio were formed in 200 μL of suspension for 15 min and adhered onto poly-L-lysine-coated glass slides (Polyprep, Sigma-Aldrich) for 10 min, all at 37°C, as described elsewhere (Banerjee et al., 2007). Fixing, permeabilization, and immunostaining for F-actin and perforin were also performed as previously described (Banerjee et al., 2007). After staining, slides were covered with 0.15 mm coverslips (VWR Scientific) using anti-fade containing mounting medium (Molecular Probes) and allowed to cure overnight at room temperature before imaging. Imaging of immunostained cells was performed using a spinning disk confocal microscope (Olympus IX-81 DSU with Hamamatsu EM-CCD camera), and all images were analyzed using Volocity software (Improvision). The *x*,*y*-plane of a given cell imaged for analysis was one in which perforin was visualized (in an NK cell), or one of near maximal diameter (in experiments without an NK cell). To evaluate F-actin localization throughout the cell volume, 10–15 images were acquired through the *z*-axis at 0.5 μm intervals and were reconstructed using Volocity software. While the spacing between x,y images in the *z*-axis was maintained constant, the number of images acquired was determined by defining z-axis limits at the top and bottom of the cell in order to ensure capture

throughout the volume of the cell. To avoid any bias that could potentially be introduced during 3-dimesnonal reconstruction by having variable numbers of images per unit volume, the 0.5 μm fixed *z*-axis intervals were utilized in all experiments. To enable quantitative analysis, detection settings (camera exposure and intensification) were adjusted for all samples so that a control antibody-stained sample was as uniformly close to background levels as possible and individual experimentally stained samples were neither saturating nor bleeding through to other fluorescent channels.

Where specified, measurements were performed to determine if lytic granules had polarized to the synapse of NK cell-target cell conjugates. Specifically, the centroid of the entire lytic granule region was determined using Volocity software and the shortest distance from the centroid to the immunological synapse was measured as previously described (Banerjee et al., 2007; Makedonas et al., 2009; Sanborn et al., 2009).

2.3) Statistical evaluations

For fixed cell microscopy, the minimum number of cells evaluated in a given experiment was determined using a sample size calculation based upon preliminary data and previously published experience with F-actin accumulation (Banerjee et al., 2007). Sample size calculations were performed using the DSS sample size calculator (DSS Research) and employing an α error (the probability of falsely accepting a sample size) and β error (the probability of falsely defining a sample size as underpowered) of 1%. For all statistical analyses of data, differences between cell types or conditions were determined using a two-tailed Student's *t* test using Excel (Microsoft). Differences were considered significant if $p<0.05$.

3) Theory/Calculation

3.1) F-actin quantitation

The purpose of our study was to develop quantitative algorithms for measuring F-actin accumulation without the need for manipulation of NK or target cells prior to conjugation. F-actin was measured at the NKIS through the use of fluorescent phalloidin, and the fluorescent signal corresponding to regions of F-actin was defined in two different ways. The first was by using a threshold of 5 standard deviations of intensity higher than the average intensity of the fluorophore within the field (5SD), and the second was by using a single value for intensity threshold that when applied to unconjugated NK cells gave a minimally detectable region ("*Fixed-intensity threshold*"). To quantify F-actin at the NKIS, the entire interface between the effector cell and the target cell conjugate was sub-divided into a series of 1 μm^2 boxes or square cuboids, each with the size of 1μm (*x*) × 1μm (*y*) × 5–7 μm (*z*). In all equations used, the number of boxes or square cuboids across each immunological synapse, "*n*", were defined as R_1,..R_n. Using either the 5SD threshold or the *fixed-intensity threshold*, the mean fluorescent intensity of the phalloidin fluorophore in the region defined (F-actin MFI) and the area or volume occupied by phalloidin (F-actin area/volume) were measured separately in each of the subregions. To determine F-actin content at the NKIS, the F-actin area/volume obtained in each of the subregions (R_1 … R_n) was multiplied by the respective mean fluorescent intensity of that particular subregion (i.e., R_1 area × R_1 intensity) and then summated as "A", where A = [(R_1 area × R_1 intensity) + (R_2 area × R_2 intensity) + … (R_n area × R_n intensity)], or A= $\Sigma_{1\ldots n}$(R area × R intensity) (Figure 1A).

3.2) Defining F-actin accumulation

In an effort to define accumulation of F-actin and contribution by NK cells, identical numbers of subregions, *n*, were also taken from the cortex of an equal number of unconjugated effector cells and unconjugated target cells. These subregions were evaluated for F-actin area/volume and intensity as explained above. The $\Sigma_{1\ldots n}$(R area × R intensity) for unconjugated target cells

was defined as “B” and for unconjugated NK cells as “C” (Figure 1B, C). To measure accumulation of F-actin at the NKIS the value of F actin contained in *n* subregions in unconjugated NK cells “C” and unconjugated target cells “B” was added together and then subtracted from “A”, which represents the F-actin contained in *n* subregions at the NKIS; NKIS F-actin accumulation = A−(B+C).

Because the area/volume and intensity of F-actin at the interface of two cells may be distinct from that in unconjugated cells, and in an effort to more specifically determine the amount of F-actin contributed by effector-target cell conjugation at the NKIS, two additional, but similar approaches were employed to estimate F-actin accumulation at the NKIS. In the first, *n* subregions were measured at the contact zone of target cell-target cell conjugates and multiplied by their intensity, in order $\Sigma_{1\ldots n}$[(R area) × R intensity] and defined as “D_1” (Figure 1D). Although this interface is often inherently larger than the NKIS due to the larger size of the target cells, the subregions measured at the target cell-target cell interface were of the same dimensions as the subregions used to generate “A”, “B”, and “C”. To estimate the content of synaptic F-actin that was contributed by as a feature of target cell-induced activation at an NK cell-target cell conjugate, the F- actin content from the target cell-target cell conjugate “D_1” was subtracted from the actin content of NKIS “A”; NKIS F-actin accumulation = A−D_1. Thus, F-actin contributed as a feature of effector and target cell conjugation = A−D_1.

Since “D_1” represents the interface of two target cells, as a second approach the F-actin accumulation at homotypic effector and target cell interfaces was included to define the F-actin specifically contributed by an NK cell at the NKIS. Here, *n* subregions were measured at the contact zone of an effector cell-effector cell conjugate, divided in half, and multiplied by their intensity, in order $\Sigma_{1\ldots n}$[(R area/2) × R intensity] and defined as “E_2”. (Figure 1E) Similarly the value for F-actin at the target cell-target cell interface “D_1”, was also divided by two prior to multiplying by the intensity, in order $\Sigma_{1\ldots n}$[(R area/2) × R intensity] and defined as “D_2” (Figure 1D). Therefore, to estimate the F-actin contributed to the NKIS as a feature of NK cell activation, the F-actin measured at an NKIS (A) was subtracted from half of the value for F-actin at an effector cell-effector cell interface (E_2) added to half of the value for F-actin at a target cell-target cell interface (D_2). Thus, F-actin accumulation at the NKIS that was contributed by NK cell activation was additionally defined as A−(D_2+E_2)

The use of NK cell-NK cell or target cell-target cell interfaces in calculations of synaptic F-actin accumulation accounts for any homotypic induction of F-actin, but does not account for any F-actin induced in the target cell, by the NK cell. Thus, an alternative set of measurements were pursued in which NK cells stably expressing a GFP-fused cell surface receptor was used to define the F-actin contained within the GFP-defined border on the NK cell side of the conjugate. Here, KIR2DL1-GFP or CD2-GFP expressing YTS cells were used to form conjugates with target cells and a fixed intensity threshold was used to define F-actin contained only within the GFP boundary of the NK cell. The F-actin content was then measured via the region-based approach described above. Using these approaches the F-actin within the GFP-defined NK cell at the NKIS was defined as “F”, while that in an equal number of regions in an unconjugated NK cell was defined as “G”. Thus, in parallel to the methods described above, synaptic NK cell F-actin content was determined as “F” and that contributed by the NK cell as a feature of synapse formation as “F-G”. These approaches were applied to KIR2DL1-GFP expressing cells.

4) Results

4.1) F-actin accumulation at the NKIS as determined by analysis of 2-dimensional confocal fluorescent images

To determine the amount of F-actin that was accumulated at the NKIS, we first developed an algorithm to estimate the total F-actin content at the NKIS based upon the area and intensity of fluorescent phalloidin signal in confocal micrographs of fixed, permeabilized and stained conjugates (Figure 1A). This region "A" was measured specifically in the mature lytic NKIS, where lytic granules (as defined by perforin staining), had polarized to the synapse (Figure 1A – right). This value was then obtained from the mature NKIS of multiple NK cell-target cell conjugates (Figure 2 – "A"). The F-actin content at the NKIS, however, was composed of the cortical F-actin of both the effector and the target cell. Thus, to estimate the F-actin that had accumulated at the NKIS as a result of target cell-induced NK cell activation, we aimed to compare the F-actin content at the NKIS to that in equal sized regions in unconjugated target cells (Figure 1B) and NK cells (Figure 1C). These regions were measured in the same number of unconjugated target and NK cells in which region "A" was measured at the NKIS (Figure 2 – "B" and "C"). To use these values to estimate F-actin accumulation at the NKIS, they were sequentially (in the order of acquisition) subtracted from those obtained for total F-actin content at the NKIS. In almost every individual calculation the remainder, i.e., the quantity of F-actin accumulated at the NKIS, was greater than the F-actin content of unconjugated effector cells (Figure 2, "A−(B+C)"). The mean of these individual values for accumulated F-actin across the multiple conjugates was also greater than the mean of the F-actin content in the similarly sized region in a similar number of unconjugated target cells or NK cells. This first algorithm represents a quantitative assessment of activation-induced F-actin accumulation at the NKIS.

A potential concern regarding this initial algorithm, however, was that two overlapping cell cortices could inherently provide a nonlinear increase in F-actin intensity or area. This could bias the estimation of F-actin accumulation at the NKIS when comparing the quantity in conjugated to unconjugated cells. Thus, to control for the increased intensity and/or area of F-actin that occurs when two cell cortices touch, and to discern that resulting from NK cell activation specifically, a second set of algorithms were developed. The specific focus of this effort was to measure the quantity of F-actin at the NKIS that was contributed by the NK cell as a specific feature of target cell-induced activation. To facilitate this approach, the amount of F-actin in the same sized region used to define the NKIS was measured at the contact zone of a target cell-target cell conjugate.. This value, "D_1", was then subtracted from the previously estimated F-actin content of the NKIS, "A" (Figure 1D, 2). An assumption in the use of "D_1", however, is that the target cell-target cell interface represents an appropriate non-activated quantity of F-actin at a cell-cell interface. It does not account for any F-actin induced in an NK cell by non-productive cell contact. Thus the amount of F-actin in the same sized region used to define "D_1" was determined at the interface observed between two NK cells. The area used to define "D_1" and this new value, however were divided in half in order enable the cumulative estimation of F-actin from a target and effector cell in a series of regions equivalent to "A" and were defined as "D_2" and "E_2", respectively (Figure 1D,E). Here, the sum of "D_2" and "E_2" were subtracted from the previously estimated F-actin content of the NKIS, "A", to provide an effector and target cell-based estimate of F-actin newly contributed to the NKIS. Similar to the first algorithm "A−(B+C)", the values for "A−D_1", or "A−(D_2+E_2)" were significantly higher than the measurement for cortical F-actin content in the similarly sized area of unconjugated NK cells "C" (Figure 2). Furthermore, there was no significant difference in the F-actin content at the NKIS as estimated by the different algorithms ("A−D_1", or "A−(D_2+E_2)" vs. "A−(B+C)", $p>0.1$), suggesting that the accumulated F-actin at the NKIS [A−(B+C)] was contributed by the NK cells and not from the target cells.

4.2) F-actin accumulation at the NKIS as determined by analysis of 3-dimensional reconstructions

Although the approach for synaptic F-actin accumulation described in section 4.1 could be applied to a single *x*,*y*-axis-oriented plane within the NKIS, any individual plane could potentially represent a disproportionate accumulation of F-actin when compared to the entire 3-dimensional face of the NKIS. Thus, it was important to consider the full contribution of cortical F-actin present throughout the *z*-axis. This was attempted using the same set of equations utilized to generate the estimates in 2-dimensions, but replacing the 1 μm^2 boxes with rectangular cuboids to define the individual regions. As an example, the same confocal micrograph evaluated in an single *x*,*y*-axis-oriented plane in Fig 1A was considered as a 3-dimensional image composed of multiple integrated *x*,*y*-axis-oriented optical sections along the *z*-axis and demonstrated compressed into a single 2-dimensional image (Fig 3A). Although the polarization of perforin to the NKIS is still evident, there is additional complexity apparent in F-actin patterning.

To determine if the measurements applied to a single plane describe a similar accumulation of F-actin when multiple planes were considered, the algorithms utilized in Fig 2 were applied to 3-dimensional reconstructions of those very cells or conjugates. Although the formulas used were the same, individual cuboidal regions having the identical *x*,*y*-axis dimensions of the squares used to measure cortical F-actin in the 2-dimensional images were employed. As for the square regions, sufficient cuboidal regions were used to cover the 3D distribution at the NKIS and the same number of regions used at the cortex of unconjugated cells, or the interface of target-target cell conjugates. Using this approach, considerable accumulation of F-actin was identified at the NKIS compared to that in unconjugated NK cells and target cells [$A-(B+C)$], as well as that at the interface between conjugated target cells (C vs. ($A-D_1$), or [$A-(D_2+E_2)$]) (Fig. 3B). The values obtained using the equations were greater than those from the 2-dimensional images, as would be expected, because greater amounts of F-actin were measured. As for the 2-dimensional analyses, there was no difference in synaptic F-actin content among the algorithms used [($A-D_1$), or $A-(D_2+E_2)$, vs. $A-(B+C)$, $p>0.1$]. Thus, in 2 or 3-dimensions, F-actin can be quantitatively similarly defined as accumulating at the NKIS.

4.3) NK cells accumulate F-actin at the lytic but not inhibitory NKIS

The ligation of NK cell inhibitory receptors can result in the formation of an inhibitory synapse that blocks further maturation of the NKIS and prevents cytotoxicity in part by preventing F-actin accumulation at the synapse (Masilamani et al., 2006). In the case of KIR2DL1, this has been attributed to a direct inhibition of the F-actin reorganization machinery by KIR2DL1 signaling (Stebbins et al., 2003). Given that we have only thus far tested our quantitative algorithms using unconjugated cells and the lytic NKIS, we next wanted to determine if our approach could discern differences in F-actin accumulation between the lytic and the inhibitory NKIS. Because, one of our algorithms [$A-(B+C)$] demonstrates the F-actin content accumulated at the IS, and the others, ($A-D_1$) and [$A-(D_2+E_2)$], F-actin more specifically account for that contributed by effector and target cell interaction, we sought to compare both of our algorithms at the inhibitory synapse, where F-actin accumulation is specifically inhibited in NK cells. We hypothesized that this would establish any contribution of F-actin by the target cell that was induced by contact with the NK cell, which could confound our algorithms. Thus, in order to address these questions and apply our approaches to discern differences in previously validated NKIS models, we chose to evaluate the effect of specific KIR2DL1 ligation upon F-actin accumulation in the YTS NK cell line.

To evaluate differences in F-actin accumulation between the lytic NKIS and the KIR2DL1-goverened inhibitory NKIS, we utilized YTS cells stably expressing a KIR2DL1-GFP fusion protein and 721.221 target cells expressing either the KIR2DL1 ligand HLA-Cw4 or the non-

cognate HLA-Cw3 (Burshtyn et al., 2000). Since YTS cells do not endogenously express KIR2DL1, the exogenously supplied receptor is responsible for ligand recognition in this system. When a KIR2DL1-GFP fusion protein-expressing YTS cell was conjugated with a target cell expressing the non-cognate HLA-Cw3, the KIR2DL1 did not cluster and F-actin appeared to accumulate at the NKIS (Fig. 4A). Consistent with the formation of a lytic NKIS, perforin also appeared polarized toward the target cell. When a KIR2DL1-GFP fusion protein expressing YTS cell was conjugated with a target cell expressing the cognate HLA-Cw4, however, the KIR2DL1 clustered at the NKIS and there appeared to be minimal F-actin accumulation (Fig 4B). Consistent with the formation of an inhibitory NKIS, perforin was not polarized toward the target cell. Since our definition of a mature lytic synapse includes the polarization of perforin, in these experiments studying the inhibitory synapse, conjugates between YTS KIR2DL1 and HLA-Cw4 cells were allowed to form for the same amount of time as those generating a mature lytic synapse.

To test our algorithms and quantitatively compare F-actin content at the lytic and inhibitory NKIS, we next applied our measurements to 2-dimensional images from multiple conjugates similar to those demonstrated in Figures 4A,B. We also evaluated multiple unconjugated YTS-KIR2DL1 cells as well as target cell-target cell conjugates in order to apply our equations ([A −(B+C)] and ($A-D_1$)). In these analyses $A-D_1$ was used instead of [$A-(D_2+E_2)$] since they were not significantly different in Figure 2 and Figure 3. When using either of the equations, we found that the content of F-actin, or contributed F-actin at the NKIS defined as the product of MFI and area was greater at the lytic NKIS than at the inhibitory NKIS (Fig 4C). In defining the F-actin region for these measurements, we used the 5SD threshold. Since 721.221 target cells have a greater F-actin content than K562 target cells, some of the brightest areas of F-actin were found in target cells. Thus, in an effort to not bias this contribution, and to include all F-actin at the NKIS contributed by the NK cell, an absolute threshold to define the F-actin region was also used by applying the *fixed-intensity threshold* (single value) approach. Here, a similar result was obtained, as both equations ([A−(B+C)] and ($A-D_1$)) demonstrated greater F-actin accumulation at the lytic NKIS (Fig. 4D). To determine the relative contributions of F-actin per unit area separately from any change in total F-actin area at the NKIS, the F-actin MFI and area were considered individually. Using either the 5SD or *fixed-intensity threshold* approach, the F-actin area (Fig 4E,F) and MFI (*fixed-intensity threshold* only - Fig. 4H) were both greater in the lytic NKIS as opposed to the inhibitory NKIS. This suggests that there were increases in both the density and depth of F-actin at the NKIS in the lytic, but not inhibitory synapse.

In some cases (most commonly when using the 5 SD threshold for defining F-actin regions), negative values for accumulation of F-actin at the inhibitory synapse were obtained (Fig 4C, E, G). One explanation for this finding could be that that the inhibitory signaling resulted in net disassembly of cortical F-actin so that less F-actin was found at an inhibitory NKIS than in the cortex of an unconjugated NK cell. Although not abrogated completely, fewer negative values were obtained when using a *fixed-intensity threshold* approach to define F-actin (Fig. 4D, F, H). This suggests that the 5SD approach for defining regions of F-actin may lead to underestimation of F-actin at the NKIS contributed by the NK cells.

4.4) NK cell surface receptor-defined evaluation of F-actin at the NKIS

Since F-actin accumulates at the NKIS in the cell cortex, it is possible to specifically determine the cortical F-actin in a conjugated NK cell by defining the NK cell surface in a conjugate. The algorithms used thus far to evaluate F-actin at the NKIS have not exploited NK cell surface definition for this purpose. One potential use of such measurements might be in other cells for which specific cell surface definition might not be feasible. In NK cells, however, there are many appropriate means for distinguishing the NK cell surface from that of the target cell.

Thus, we developed an additional set of measurements aimed at specifically measuring F-actin on the NK cell side of the synapse. Since YTS KIR2DL1-GFP cells were used in prior experiments, we now evaluated the F-actin within the NK cell within the GFP boundary. The F-actin contained within 1μm^2 regions in the GFP-delimited NK cell were measured as described for measurement "A", but because they are only comprised of NK cell F-actin are now defined as "F" (Figure 5A). To generate an estimate of the F-actin contributed by the NK cell to the IS (analogous to [A-(B+C)]), we measured the F-actin within the GFP boundary in an unconjugated NK cell, "G" (Figure 5A), and subtracted this from "F". This analysis was performed using a fixed intensity threshold in multiple conjugates between YTS KIR2DL1-GFP cells and 721.221 cells expressing either HLA-Cw3 or HLA-Cw4, as described in section 3.1. The F-actin accumulation (Figure 5B) as well as F-actin MFI (Figure 5C) and F-actin area (Figure 5D) all yielded similar values to those obtained using either the ([A−(B+C)], or (A −D_1) equations used in Figure 4. This additionally demonstrated that F-actin accumulates preferentially at the lytic as compared to the inhibitory NKIS, the significance of which can be characterized by the polarization of the lytic granules at the lytic, but not at the inhibitory NKIS (Figure 5E). Furthermore, these approaches also validate our non-surface delimited evaluation of F-actin at the NKIS in YTS-KIR2DL1 cells and therefore suggest that either approach is likely appropriate for determining synaptic F-actin content.

To ensure that the results obtained using a GFP-delimited approach in YTS KIR2DL1-GFP cells were not specific to the use of KIR2DL1-GFP, we performed a similar evaluation of the lytic synapse using YTS CD2-GFP cells. In these experiments we also used two different target cells in parallel in an effort to validate the hypothesis that F-actin accumulation at the NKIS should be measurable with any target cell susceptible to NK cell cytotoxicity. Thus, we used either 721.221 cells or K562 cells stably expressing CD86 (Banerjee et al., 2007), both of which can be killed by YTS CD2-GFP cells. When F-actin amount at the NKIS in the GFP defined NK cell was measured as "F" it was significantly greater than the F-actin found at the homotypic target cell interface, "D_1" (Figure 6B). The same significant differences were identified for F-actin area and MFI (Figure 6 C,D). A significant difference between "F" and "D_1" was also found in the YTS KIR2DL1-GFP cells forming a lytic synapse with 721.221 HLA-Cw3 cells shown in Figure 4, but not at inhibitory synapses formed with 721.221 HLA-Cw4 cells (data not shown). The F-actin content in unconjugated YTS CD2-GFP cells, "G", was negligible relative to F and thus not used. These differences between "F" and "D_1" in YTS CD2-GFP cells were found with both target cell lines used. F-actin accumulation in the NK cells as induced by the different target cells, however, was discerned and may represent a specific characteristic of these synapses that can be reproducibly detected using these approaches.

5) Discussion

5.1) Quantitative assessment of F-actin accumulation at the NKIS

NK cells accumulate F-actin at the activating NKIS as an early step in generating the lytic NKIS (Orange, 2008). Algorithms for quantitatively measuring the F-actin content at the NKIS, however, are not standardized. In particular, it has been difficult to obtain an objective measurement of F-actin accumulation at the NKIS without introducing a fluorescent biosensor of some type into either the NK cell or target cell prior to forming conjugates. This is important as prior manipulation of the cells to be conjugated has the potential to affect physiological F-actin dynamics and creates the need for experimental manipulations that may not be feasible in all experimental systems. While approaches not utilizing a specific receptor on an NK or target cell were not expected to be inherently superior, they were pursued as a potentially useful additional tool in quantitative assessment of the NKIS. Thus, we developed and evaluated algorithms for estimating F-actin content at the NKIS formed by otherwise unmanipulated NK and target cells.

The first algorithm was intended to measure F-actin accumulation at the NKIS, and the second to discern F-actin accumulated at the NKIS contributed by the NK cell above that occurring in non-productive interactions. While both approaches represent estimates, they were able to reproducibly identify increased F-actin at the NKIS compared to that in the cortex of unconjugated cells, and homotypic conjugates as well as that found at the inhibitory NKIS. Given the quantitative nature of these evaluations, it is likely that they will be applicable to evaluating the effects of more subtle experimental interventions upon F-actin reorganization at the NKIS. As this represents a critical step in NKIS formation and function (Orange et al., 2003; Masilamani et al., 2006), it is likely that this type of quantitative assessment will be useful in studying integration of signals from various receptor inputs that combine to either promote or restrain lytic function. Since the contributions of individual signals may not represent “all or none” effects upon F-actin accumulation at the NKIS, simple methods for quantitation will be instrumental.

The methods utilized in this work have a number of limitations. First, they are only relative estimates and rely upon differences in fluorescence intensity of fluorophore-conjugated phalloidin, which at least under certain circumstances may not necessarily be linear (Huang et al., 1992). Second, they fail to account for any newly polymerized actin in the target cell that would be specifically induced by binding to an NK cell. In an effort to partially address these, we compared the lytic and inhibitory NKIS using a well-established NK cell model system. Here, we were able to reproducibly measure differences in F-actin accumulation despite the likely non-linearity of fluorescent signals. We also did not find substantial F-actin accumulation at the inhibitory NKIS, as the calculations defined means very close to zero. Were there to be F-actin accumulation contributed by the target cell in an NK cell-target cell conjugate, positive values for accumulation would have been expected. While this does not exclude the possibility of target cell-contributed F-actin, it demonstrates that this contribution is as at least minor in comparison to that contributed by the NK cell.

In an effort to address target cell contributed F-actin, we also developed and contrasted similarly developed algorithms that utilize a fluorescent receptor expressed in the NK cell to define the F-actin content specifically within the NK cell (Figure 5,6). These approaches yielded similar results and at least in part validated the non-receptor dependent algorithms. They also present an alternative approach for the estimation of F-actin accumulation at the NKIS.

The algorithms used were also compared in 2- and 3-dimensions using the same cells studied in either a single confocal plane or throughout their z-axis. Although it is likely that highly relevant variations will exist throughout the full 3-dimensonal face of the NKIS, the evaluation of accumulation in the single *x*,*y* plane did demonstrate similar degrees of F-actin accumulation compared to the evaluation in 3-dimesnions. Thus, while not a replacement for 3-dimensional reconstruction of the NKIS, quantitative assessment of 2-dimensional planes would seem to provide a reasonable surrogate.

The algorithms were also applied to synapses formed with effector and target cells that have similar or different quantities of F-actin. Specifically, K562 cells have an MFI of F-actin similar to *ex vivo* NK cells ($p=0.83$; not shown), while the MFI of F-actin in 721.221 cells is significantly greater than in YTS cells ($p=0.02$; not shown). Thus, the algorithms can be used to evaluate F-actin accumulation at the synapse even when the target cell possesses abundant F-actin at baseline. This situation, in particular, presents a challenge in attempting to discern more subtle changes in accumulation, which might not be appreciated without quantitation. In this light, differing quantities of F-actin were detected in YTS cells conjugated with each of two different target cells (Figure 6). This may relate to specific characteristics of the target cell inducing of NK function and the detection is likely a feature of the sensitivity in measurement.

These types of approaches, therefore, may enable specific mechanistic studies of the appearance and relevance of differences in F-actin accumulation.

Finally, the utility of the algorithms for measuring F-actin accumulation required the appropriate configuration of microscope and camera settings. This necessitated the use of negative and positive controls and careful consideration of microscope-related variables. This subject has been reviewed in some detail, but it must be underscored that without rigorous calibration, accurate and meaningful data would not be possible

5.2) Applicability of algorithms to other molecular accumulations

While not specifically evaluated in this work, it is likely that the algorithms for quantitating molecular accumulation of F-actin at a cell-cell interface should be applicable to other molecules detected in fixed cells using fluorescent probes. The approaches should be especially useful for molecules that may be expressed by both cells in the conjugate. An example would be cytoskeletal elements or adhesion molecules in conjugates formed between two different types of hematopoietic cells. The approaches developed in this work would also allow an estimate of what amount of the fluorescently labeled molecule is contributed by the effector cell when its activation is induced by a target cell. This degree of accuracy, however, would depend upon the availability of established negative biological controls, such as the inhibitory NKIS used in this work (Figure 4, 5). In this case, if reproducible values for accumulation are found when the effector cell is not be expected to have molecular accumulation, then further evaluation of effector cell-induced molecular accumulation in the target cell would be indicated.

The approach and algorithms presented could also be useful in the setting of numerically evaluating the accumulation of molecules expressed in only one of the two cells in a cell-cell conjugate. While this may seem unnecessary, the use of rigorous quantitative microscopy can help prevent any artifactual contribution of fluorescence from target cells and allow for a definitive assessment of the accumulated fluorophore. Additional accuracy in measurement may prove to be important in understanding degrees of molecular accumulation that may be only partially affected by experimental intervention. In immune cell interactions this may be required to fully comprehend the evolving signal integration required for the generation of an immunological synapse.

5.3) Conclusion

In this work, algorithms intended to facilitate the quantitative assessment of F-actin accumulation at the NKIS were developed. One evaluates the accumulation of F-actin at the NKIS and the other specifically attempts to estimate the F-actin contributed by NK cell activation in the conjugate. The algorithms were demonstrated in both 2- and 3- dimensions and provided similar data regarding accumulation. They were validated using fluorescent fusion protein-conjugated NK cell receptors and were also applied to compare F-actin accumulated at the lytic NKIS relative to that at the inhibitory NKIS. Using an experimental system in which the only variable was the inhibitory receptor ligand, a significant difference was found between the quantity of F-actin at the two synapses as well as that contributed by the NK cell. Importantly, these methods were specifically developed to allow evaluation of F-actin accumulation in cells that had not otherwise been manipulated prior to conjugation and fixation. Hopefully the use of these approaches will enable highly quantitative evaluations of the NKIS, as well as the measurement of more subtle experimental effects upon NKIS formation.

Abbreviations used

F-actin	filamentous actin
KIR	Killer cell immunoglobulin-like receptor
mAbs	monoclonal antibodies
MTOC	microtubule organizing center
NK	natural killer
NKIS	NK cell immunological synapse
SMAC	supramolecular activation cluster

Acknowledgments

The authors would like to acknowledge Keri Sanborn and Gregory Rak for critical assistance with the manuscript. Paul Hallberg from the University of Pennsylvania cell sorting facility for sorting YTS CD2-GFP cells. The work was supported by NIH R01 AI-067946

References

Almeida CR, Davis DM. Segregation of HLA-C from ICAM-1 at NK cell immune synapses is controlled by its cell surface density. J Immunol 2006;177:6904–6910. [PubMed: 17082605]

Banerjee PP, Pandey R, Zheng R, Suhoski MM, Monaco-Shawver L, Orange JS. Cdc42-interacting protein-4 functionally links actin and microtubule networks at the cytolytic NK cell immunological synapse. J Exp Med 2007;204:2305–2320. [PubMed: 17785506]

Borszcz PD, Peterson M, Standeven L, Kirwan S, Sandusky M, Shaw A, Long EO, Burshtyn DN. KIR enrichment at the effector-target cell interface is more sensitive than signaling to the strength of ligand binding. Eur J Immunol 2003;33:1084–1093. [PubMed: 12672075]

Burshtyn DN, Shin J, Stebbins C, Long EO. Adhesion to target cells is disrupted by the killer cell inhibitory receptor. Curr Biol 2000;10:777–780. [PubMed: 10898979]

Davis DM, Dustin ML. What is the importance of the immunological synapse? Trends Immunol 2004;25:323–327. [PubMed: 15145322]

Fassett MS, Davis DM, Valter MM, Cohen GB, Strominger JL. Signaling at the inhibitory natural killer cell immune synapse regulates lipid raft polarization but not class I MHC clustering. Proc Natl Acad Sci U S A 2001;98:14547–14552. [PubMed: 11724921]

Huang ZJ, Haugland RP, You WM. Phallotoxin and actin binding assay by fluorescence enhancement. Anal Biochem 1992;200:199–204. [PubMed: 1595896]

Liu D, Bryceson YT, Meckel T, Vasiliver-Shamis G, Dustin ML, Long EO. Integrin-dependent organization and bidirectional vesicular traffic at cytotoxic immune synapses. Immunity 2009;31:99–109. [PubMed: 19592272]

Makedonas G, Banerjee PP, Pandey R, Hersperger AR, Sanborn KB, Hardy GA, Orange JS, Betts MR. Rapid up-regulation and granule-independent transport of perforin to the immunological synapse define a novel mechanism of antigen-specific CD8+ T cell cytotoxic activity. J Immunol 2009;182:5560–5569. [PubMed: 19380804]

Masilamani M, Nguyen C, Kabat J, Borrego F, Coligan JE. CD94/NKG2A inhibits NK cell activation by disrupting the actin network at the immunological synapse. J Immunol 2006;177:3590–3596. [PubMed: 16951318]

Orange JS. Formation and function of the lytic NK-cell immunological synapse. Nat Rev Immunol. 2008

Orange JS, Harris KE, Andzelm MM, Valter MM, Geha RS, Strominger JL. The mature activating natural killer cell immunologic synapse is formed in distinct stages. Proc Natl Acad Sci U S A 2003;100:14151–14156. [PubMed: 14612578]

Sanborn KB, Rak GD, Maru SY, Demers K, Difeo A, Martignetti JA, Betts MR, Favier R, Banerjee PP, Orange JS. Myosin IIA associates with NK cell lytic granules to enable their interaction with F-actin and function at the immunological synapse. J Immunol 2009;182:6969–6984. [PubMed: 19454694]

Stebbins CC, Watzl C, Billadeau DD, Leibson PJ, Burshtyn DN, Long EO. Vav1 dephosphorylation by the tyrosine phosphatase SHP-1 as a mechanism for inhibition of cellular cytotoxicity. Mol Cell Biol 2003;23:6291–6299. [PubMed: 12917349]

Wulfing C, Purtic B, Klem J, Schatzle JD. Stepwise cytoskeletal polarization as a series of checkpoints in innate but not adaptive cytolytic killing. Proc Natl Acad Sci U S A 2003;100:7767–7772. [PubMed: 12802007]

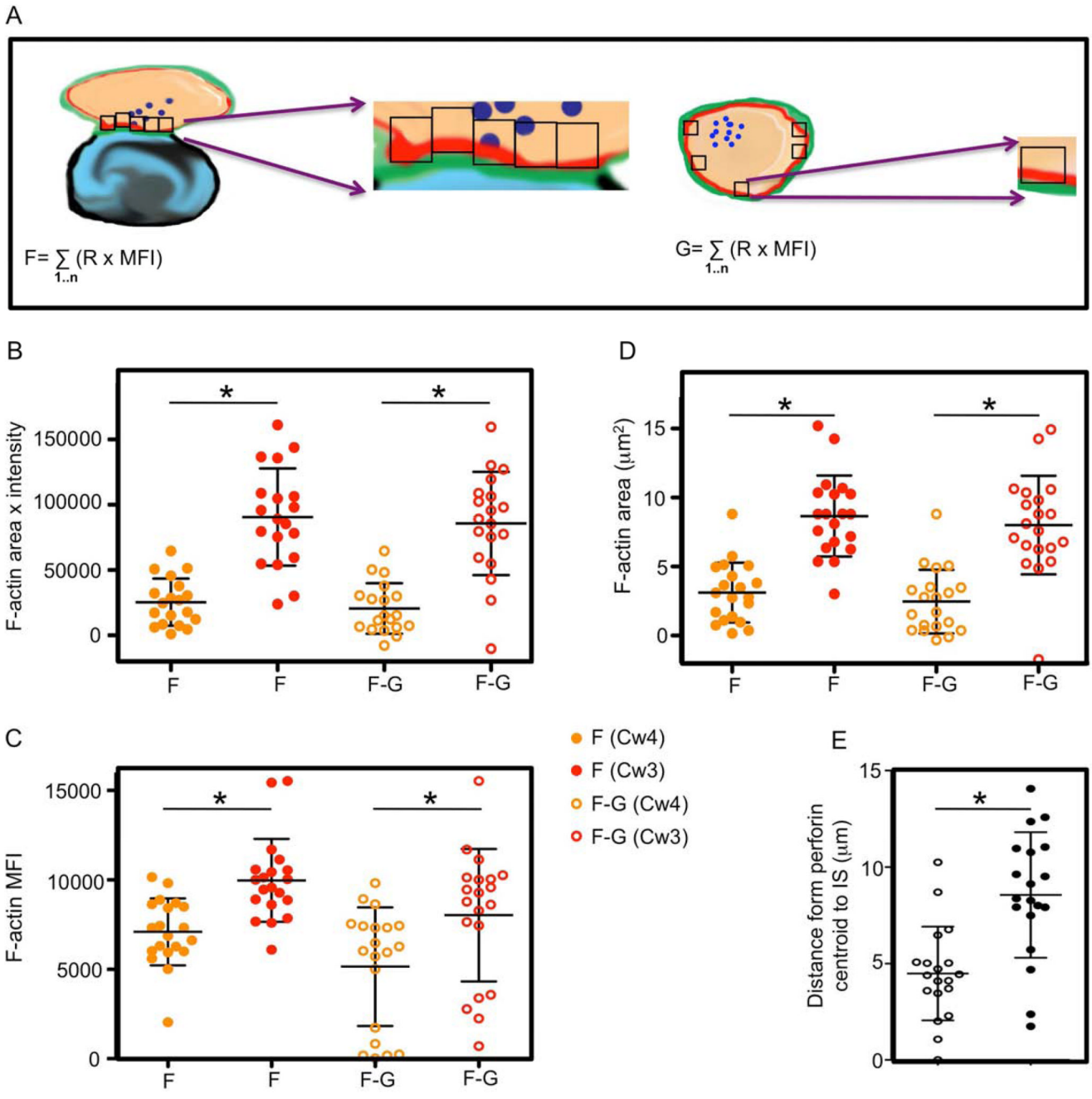

Figure 1. Two different algorithms for the evaluation of F-actin accumulation at the NKIS

NK cells conjugated with K562 target cells **(A)**, unconjugated target cells **(B)**, unconjugated NK cells **(C)**, K562-K562 target cell conjugates **(D)**, and NK cell-NK cell effector cell conjugates **(E)** were fixed, permeabilized and stained with AlexaFluor 568-conjugated phalloidin to allow detection of F-actin. Whenever present, effector cells were identified by staining with FITC conjugated anti-perforin antibody.

(A) The interface of an NK (effector) cell and a target cell conjugate was subdivided into a series of 1 μm^2 boxes demonstrated schematically (left). The area of F-actin in each box was measured by including all fluorescent signal that was 5SD above the AlexaFluor 568 MFI of the entire image (denoted R1, R2, …Rn). Using this threshold, the MFI of the AlexaFluor 568

in each of the regions was also measured (denoted MFI1, MFI2, …MFIn). The F-actin area within each subregion was multiplied by the AlexaFluor 568 MFI of the respective region to obtain an estimate of phalloidin fluorophore contained within that region (R × MFI). The product of R and MFI for each of the subregions was summated to provide a total estimate of F-actin at the NKIS in the defined regions (denoted as "A"). A representative conjugate between a human *ex vivo* NK cell (top) and a K562 cell (bottom) evaluated by differential interference contrast (DIC) and by 2D confocal microscopy demonstrate fluorescent detection of perforin using FITC-conjugated anti-perforin antibody (light blue) and F-actin using AlexaFluor-conjugated phalloidin (red) (A – Right). This conjugate demonstrates a lytic NKIS, as perforin was directed toward the interface. An overlay of all fluorescent channels is also shown. Although an *x,y* plane was selected in the *z*-axis to highlight the F-actin at the NKIS, disproportionate accumulation of F-actin in other *x,y* planes was not found. Scale bars in all images = 5μm.

(B) The cortex of an unconjugated target cell was randomly overlaid with the same number of $1\mu m^2$ subregions used to define "A" (left). F-actin area, MFI and their product were determined (denoted as "B"), as described above to define "A". Representative images of a K562 cell (DIC – left) that was also stained with AlexaFluor 568 phalloidin to demonstrate F-actin localization (red) as shown by 2D confocal imaging (right).

(C) The cortex of an unconjugated *ex vivo* NK cell was randomly overlaid with an equal number of $1\mu m^2$ subregions used to define "A" as described above (left). F-actin area, MFI and their product determined (denoted as "C"), as described for "A". Representative images of an unconjugated *ex vivo* NK cell (DIC – left) that was also stained with AlexaFluor 568 phalloidin to demonstrate F-actin localization (red) and FITC-anti perforin (light blue) as shown by 2D confocal imaging (right). The rightmost image demonstrates an overlay of all fluorescent channels.

(D) The cortex of two conjugated target cells were randomly overlaid with the same number of $1\mu m^2$ subregions at the cell-cell interface that were used to define "A" (left). F-actin area, MFI and their product were determined (denoted "D_1"), as described above to define "A". Half of the area from each of the subregions was multiplied by its respective MFI to give the product "D_2". Representative images of a K562-K562 cell conjugate (DIC – left) that was also stained with AlexaFluor 568 phalloidin to demonstrate F-actin localization (red) as shown by 2D confocal imaging (right).

(E) The cortex of two conjugated effector cells were randomly overlaid with the same number of $1\mu m^2$ subregions at the cell-cell interface that were used to define "A" (left). Half of the area from each of these subregions was multiplied by its respective MFI, and the product was denoted as "E_2"), as described above to define "A". Representative images of an NK cell-NK cell conjugate (DIC – left) that was also stained with AlexaFluor 568 phalloidin to demonstrate F-actin localization (red), and FITC-conjugated anti-perforin (light blue) as shown by 2D confocal imaging (right). The rightmost image demonstrates an overlay of all fluorescent channels.

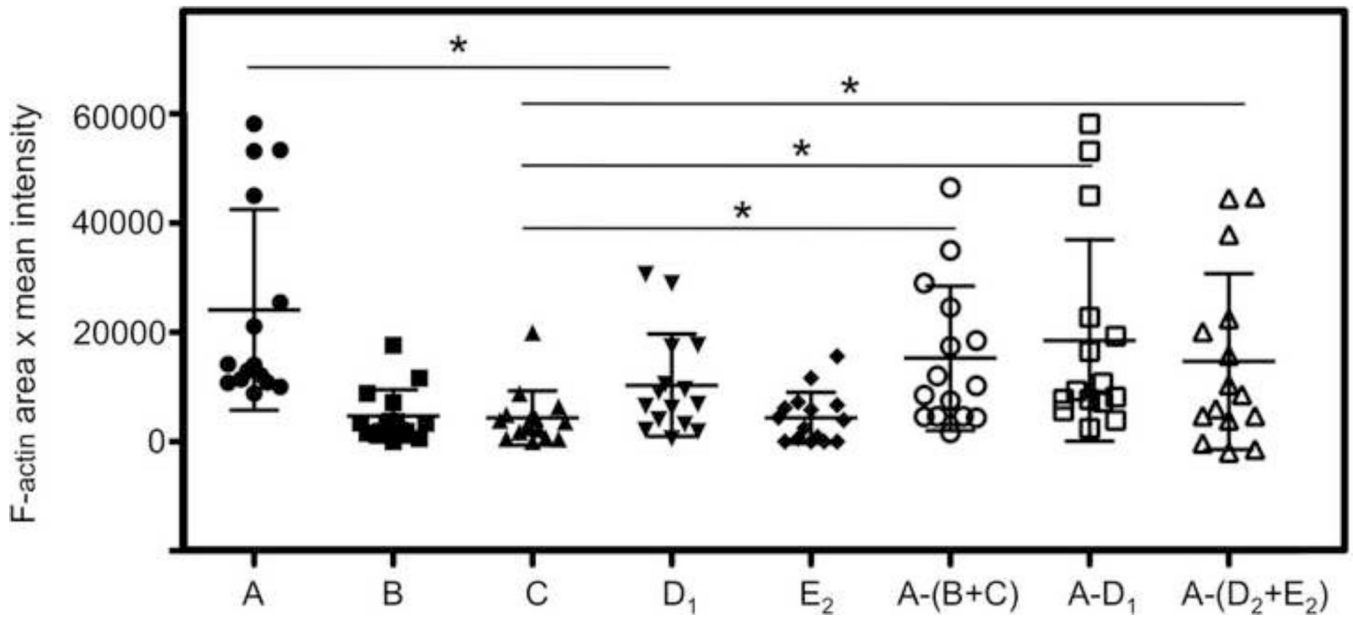

Figure 2. Estimation of F-actin accumulation at the NKIS in 2-dimensions

Each of the products defined in Figure 1, "A", "B", "C", "D_1", "D_2", and E_2 " were measured in 15 separate examples and plotted. The horizontal line in each scatter plot demonstrates the mean, and the vertical bar demonstrates the SD for each series of measurements. As described in the text, the accumulation of F-actin at NKIS was estimated by subtracting the sum of the values for F-actin content of an unconjugated target cell "B" and an unconjugated effector cell "C" from the F-actin content of the NKIS "A", or [A-(B+C)] and the calculated values were plotted. Similarly, the F-actin content at the NKIS contributed by the NK cell was estimated by subtracting the quantity defined at a target cell:target cell conjugate "D_1" from the F-actin content of NKIS "A" ($A-D_1$). Alternatively, the F-actin content at the NKIS contributed by the NK cell was calculated by subtracting the sum of half of the F-actin content at the target cell:target cell conjugate "D_2" and half of the F-actin content at an NK cell:NK cell conjugate "E_2", from the F-actin content of NKIS "A" $\{A-(D_2+E_2)\}$. Differences between values obtained for F-actin content of "A" vs. "D_1","C" vs. $\{A-(B+C)\}$, "C" vs. $(A-D_1)$, and "C" vs. $\{A-(D_2+E_2)\}$ were significant, *=$p<0.05$.

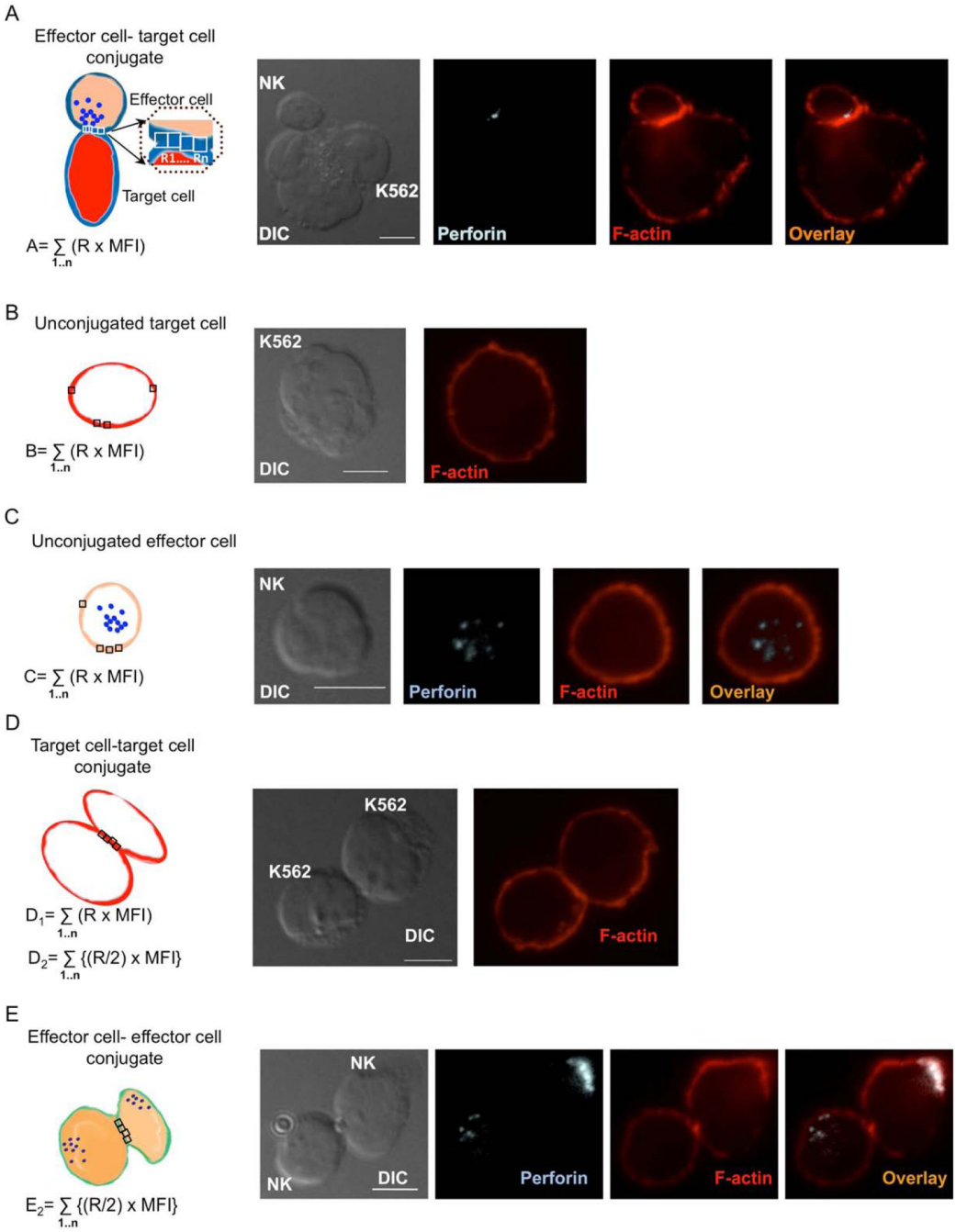

Figure 3. Estimation of F-actin accumulation at the NKIS in 3-dimensions

(A) A 3-dimensonal reconstruction of a series of confocal images collected through the *z*-axis compressed into a single image of the same *ex vivo* NK cell (top) and K562 cell (bottom) shown in Figure 1. Fluorescent detection of perforin using FITC-conjugated anti-perforin (light blue) and F-actin using AlexaFluor 568-conjugated phalloidin (red) are demonstrated. The 3-dimensional orientation is shown on the left and an overlay of all fluorescent channels on the right.

(B) Using rectangular cuboids having *x*,*y* dimensions of 1μm instead of squares, the same regions defined for 2-dimesnsions in Figure 1 ("A", "B", "C", "D_1","D_2", and "E_2") were measured in the same 15 cells measured in that figure. Similarly, the accumulation of F-actin

at NKIS was estimated as demonstrated in Figure 2 but in 3-dimensons. The horizontal bar in each series of the scatter plot represents the mean and vertical bars represent the SD. Differences between the values obtained for F-actin content in 3-dimensons of “A” vs. “D_1”,”C” vs. {A−(B+C)}, “C” vs. (A−D_1), and “C” vs. {A−(D_2+E_2)} were significant, *=p<0.05.

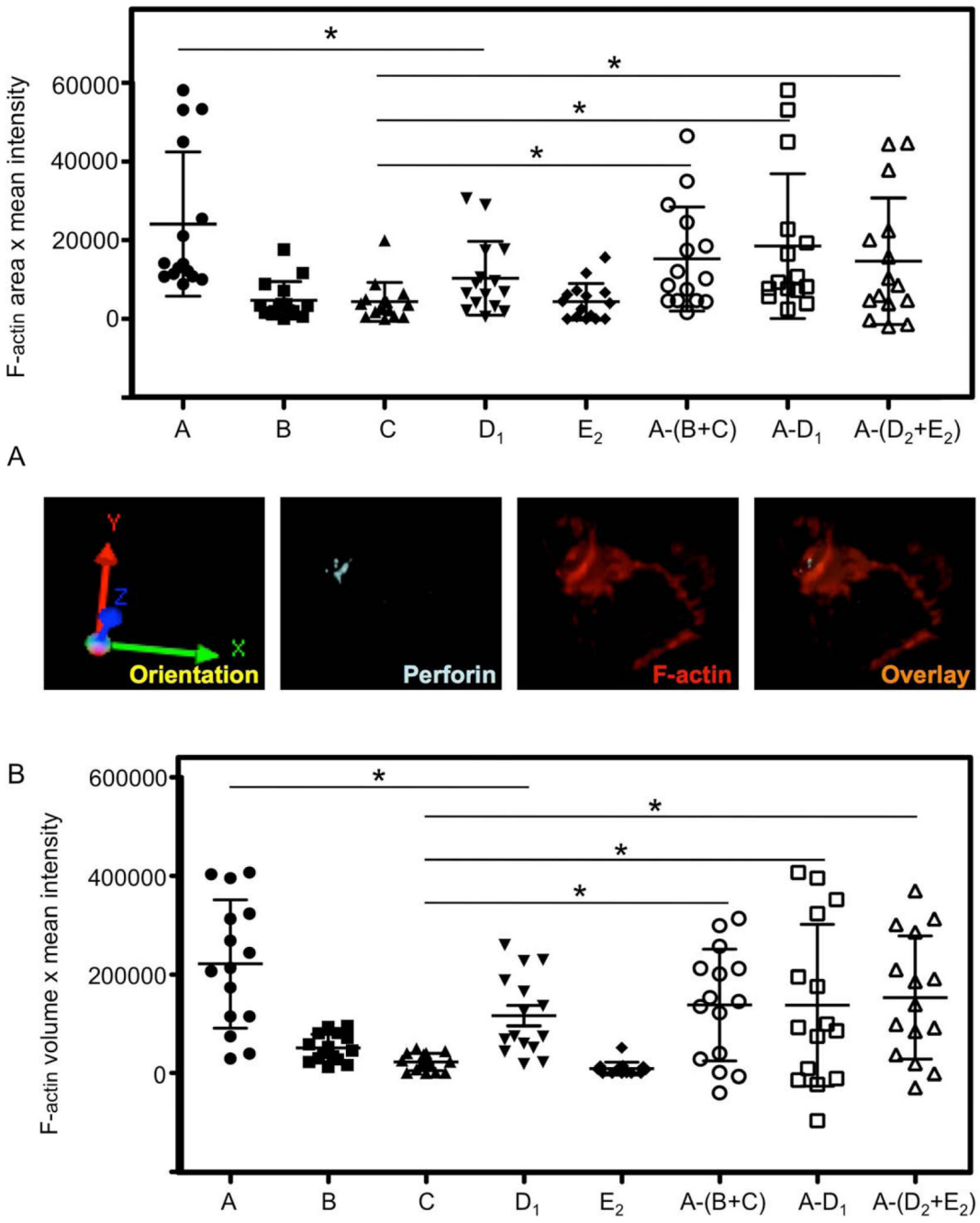

Figure 4. Quantitative effect of inhibitory signaling on F-actin accumulation at the NKIS

(A) Representative cytolytic NKIS formed between a YTS-KIR2DL1-GFP cell (top) and a non-cognate ligand-expressing 721-Cw3 cell (bottom) evaluated using DIC (left) and 2D confocal microscopy (right). KIR2DL1-GFP (green), perforin (light blue) and F-actin (red) localization are individually demonstrated along with an overlay of all fluorescent channels. Scale bars = 5μm.

(B) Representative inhibitory NKIS formed between a YTS-KIR-2DL1-GFP cell (top) and a cognate ligand-expressing 721-Cw4 cell (bottom) imaged using DIC (left) and by 2D confocal microscopy with fluorescent representations the same as in A, above (right).

(C–H) Quantitative measurements described in Figure 1 ("A", "B", "C", and "D_1") were applied to calculate the estimates of F-actin content of the NKIS, [A−(B+C)] and F-actin at the NKIS contributed by the NK cell, ($A-D_1$), at the cytolytic (black dots) and inhibitory (gray dots) NKIS. 20 unique synapses were measured and error bars represent the SD. The 5SD (C, E, G) and fixed intensity threshold (D, F, H) methods for defining F-actin regions were applied independently as two distinct approaches to define F-actin. In addition to the calculated F-actin values (C,D), the F-actin area (E,F) and MFI (G,H) are separately depicted. Comparisons of mean data between the cytolytic and inhibitory NKIS were made, and were significant, *=$p<0.05$.

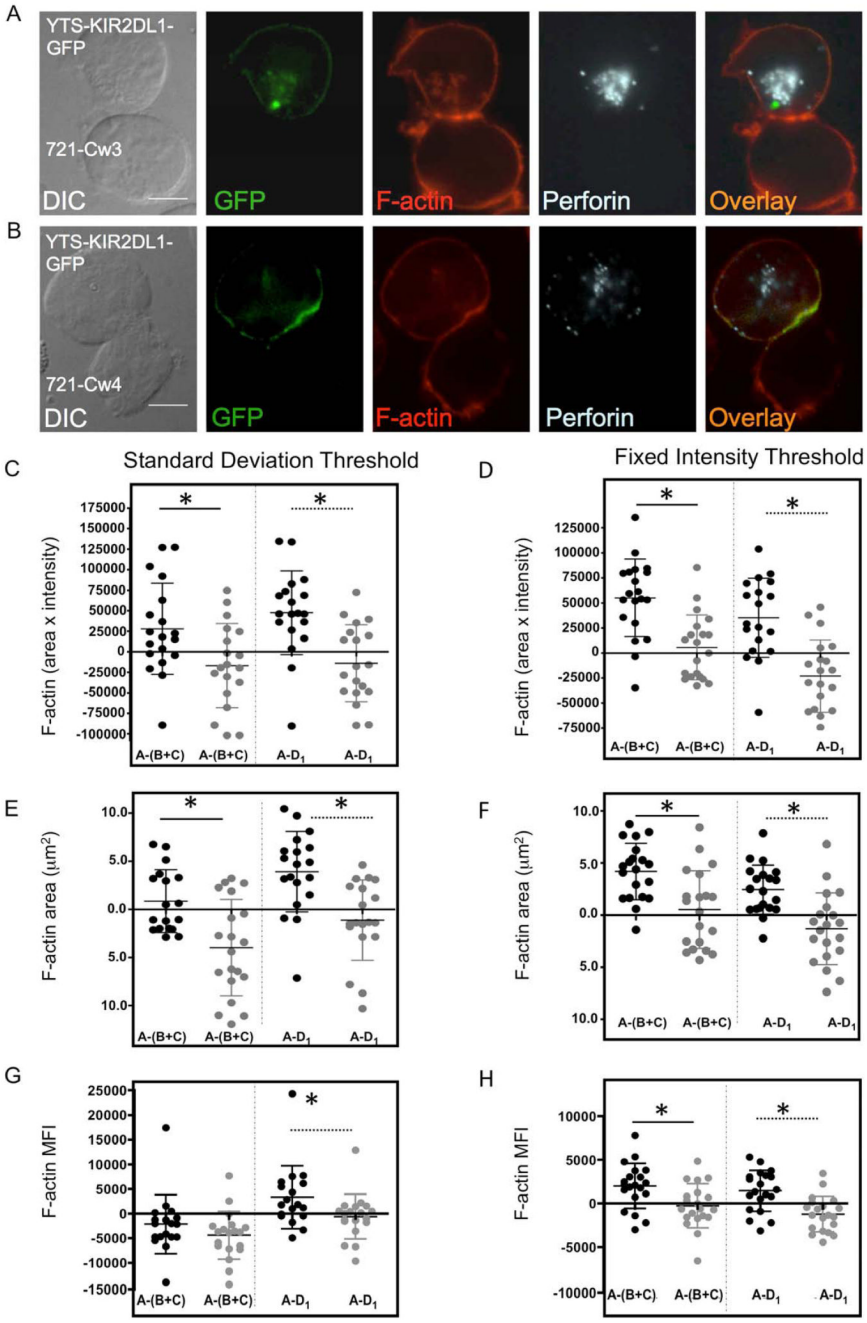

Figure 5. NK cells accumulate F-actin at the activating NKIS internal to cell-surface receptor defined NK cell periphery

(A) F-actin at the NKIS contributed by NK cells was measured by generating a series of 1 um^2 subregions across the NKIS to evaluate only F-actin selected to be within the KIR2DL1-gfp defined periphery of YTS cells. The F actin content in these subregions ("F") was measured using the same fixed intensity threshold (left) as in Figure 4. The F-actin content inside the KIR2DL1-gfp defined periphery of unconjugated YTS cells ("G") was measured by using the same intensity threshold and same number of 1μm^2 subregions used to define "F" (right). **(B–D)** F-actin content (B), MFI (C) and area (D), were measured inside the inhibitory (orange circles), and cytolytic (red circles) NKIS.. Each measurement displays 19 individual cells, the

horizontal bar in each series represents the mean and the vertical error bars the SD. The amount (solid circles – "F"), or NK cell accumulation (open circles – "F-G") of F-actin at the NKIS that was in YTS-KIR2DL1 cell within its KIR2DL1-GFP-defined surface was calculated for the inhibitory and cytolytic NKIS. Differences between values for F-actin of the cytolytic and inhibitory NKIS were significant,*=$p<0.05$.

(E) Distance from the centroid of the grouped perforin region to the IS in YTS KIR2DL1:721.221 Cw3 conjugates (open circles) and YTS KIR2DL1:721.221 Cw4 conjugates (closed circles) is shown. The mean of all individual cell measurement (n=19 cells each) is represented by a horizontal bar within each series and the vertical bar demonstrates the SD. The difference between the perforin centroid to the IS in inhibitory and cytolytic conjugates was significant, *=$p<0.05$.

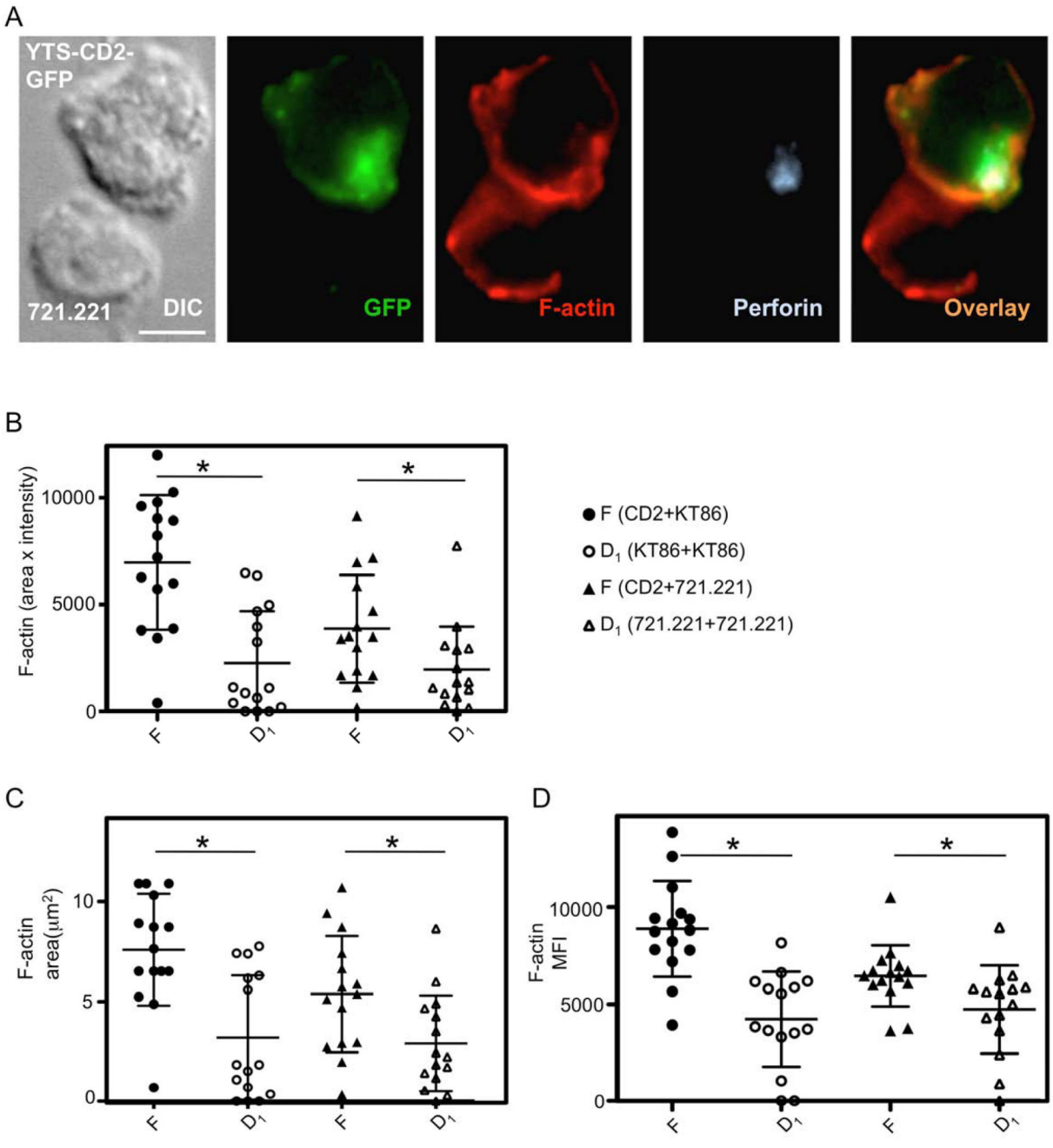

Figure 6. Validation of NK cell mediated F-actin accumulation quantitation at the NKIS upon conjugation with different target cells

(A) A representative cytolytic conjugate between a YTS CD2–GFP cell (top) and a 721.221 cell (bottom) evaluated by DIC microscopy (left) and fluorescence confocal microscopy (right) showing CD2-GFP (green), F-actin (red) and perforin (light blue). The rightmost image demonstrates an overlay of all fluorescent channels (scale bar=5μm).

(B–D) Quantitative measurements as described for Figures 1A and Figure 5A were applied to calculate F-actin content (B), F-actin area (C), and F-actin MFI (D) at the NKIS inside the CD2-GFP defined periphery of YTS CD2-GFP:KT86 cell conjugates (filled circles), and YTS CD2-GFP:721.221 cell conjugates (filled triangles). The accumulation of F-actin at KT86

cell:KT86 cell interfaces (open circles) and 721.221 cell:721.221 cell interfaces (open triangles) was also measured. For each measurement 15 cells were evaluated. Differences between values obtained for F-actin content of “F” vs. “D_1” for both type of effector-target cell conjugates was significant *=$p<0.05$.